A Method for the Evaluation of Radiation Q Based on Modal Approach

Miloslav Capek, *Student Member, IEEE*, Pavel Hazdra, *Member, IEEE*, and Jan Eichler, *Student Member, IEEE*

Abstract—A new formula for the evaluation of the modal radiation Q factor is derived. The total Q of selected structures is to be calculated from the set of eigenmodes with associated eigen-energies and eigen-powers. Thanks to the analytical expression of these quantities, the procedure is highly accurate, respecting arbitrary current densities flowing along the radiating device. The electric field integral equation, Delaunay triangulation, method of moments, Rao-Wilton-Glisson basis function and the theory of characteristic modes constitute the underlying theoretical background. In terms of the modal radiation Q, all necessary relations are presented and the essential points of implementation are discussed. Calculation of the modal energies and Q factors enable us to study the effect of the radiating shape separately to the feeding. This approach can be very helpful in antenna design. A few examples are given, including a thin-strip dipole, two coupled dipoles a bowtie antenna and an electrically small meander folded dipole. Results are compared with prior estimates and some observations are discussed. Good agreement is observed for different methods.

Index Terms—Antenna theory, eigenvalues and eigenfunctions, electromagnetic theory, Q factor.

I. INTRODUCTION

THE radiation Q factor has long been discussed as one of the most significant and interesting parameter of the radiating system, especially in the field of the electrically small antenna (ESA) theory [1]. Each radiating shape has a minimum possible Q which is related to the maximum possible bandwidth potential [2].

There are many methods for estimating Q approximately (chronologically Wheeler [3], Chu [4], Harrington [5], Collin and Rotschild [6], McLean [7], Geyi [8]). Earlier work [3]–[7] do not consider actual current distribution, so they have to deal only with bounds related to dimensions of the enclosing sphere. The first attempt to include source distribution (current/charge) was presented by Geyi [8], but these energies are still quasistatic. Different approach taking the actual shape into account (based on static polarizability), was presented by Gustafsson *et al.* [9].

For effective ESA design as well as for the rigorous study of radiating structures, it is appropriate to use the calculation method based directly on the sources (currents), respecting their topology. These requirements have been fulfilled by G. Vandenbosch [10]. The derived expressions are rigorous, widely usable and easy to implement. They have been verified and successfully tested for simple examples in [11].

We extend this theory for modal analysis purposes, based on the theory of characteristic modes (TCM) [12] and then utilize them for the investigation of radiation Q for some canonical antennas. This approach allows us to study the behaviour of the shape of the radiating structure and its feeding separately. This means that the modal quantities have only to be calculated once and then the effect of the feeding port on superposition is studied through the coupling matrix, later denoted as $\boldsymbol{\beta}$. In addition, understanding the behaviour of modal energies assists in effective ESA design as will be shown in the case of optimization of the meander folded dipole.

The main objective of this paper is to derive the expression for the summation of modal energies and powers in order to obtain total Q. The comparison between the final expressions (24), (25) and some estimations of Q are given in Section V. All algorithms were coded in Matlab R2011a and employed in our in-house antenna tool. The described method could be used for arbitrary (triangularized) surface antennas with air dielectric.

II. THE RADIATION Q-FACTOR

The radiation Q factor is usually defined for antennas as [1]

$$Q = \frac{2\omega_0 \max\{W_e, W_m\}}{P_r}, \tag{1}$$

where W_e and W_m are the time averaged stored electric and magnetic energies and P_r is radiated power. The (1) assumes that the antenna is tuned to the resonance at angular frequency ω_0 by an ideal lossless reactive element so that the input impedance is pure real, [6]. Moreover, it is known that Q is inversely proportional to the antenna (fractional) bandwidth and for the constant VSWR $< s$

$$\text{FBW} \approx \left(\frac{s-1}{\sqrt{s}}\right)\frac{1}{Q}, \tag{2}$$

where the Q factor in (2) is assumed to be much greater than one.

The following expressions for W_e, W_m and P_r are analytically derived in [10] and generalized to a suitable form for the sake of the proposed method (note that the indexes u and v will be associated with the mode indexes in subsequent sections)

$$W_e^{u,v} = \frac{1}{16\pi\omega_0^2\epsilon_0}\left(I_{W_e}^{u,v} - I_{W_r}^{u,v}\right) \tag{3}$$

and

$$W_m^{u,v} = \frac{1}{16\pi\omega_0^2\epsilon_0}\left(I_{Wm}^{u,v} - I_{Wr}^{u,v}\right) \qquad (4)$$

where

$$I_{We}^{u,v} = \int\limits_{\Omega_1}\int\limits_{\Omega_2} q_u(\mathbf{r_1})q_v^*(\mathbf{r_2})\frac{\cos(k_0 r_{21})}{r_{21}}\mathrm{d}\Omega_1\mathrm{d}\Omega_2, \qquad (5)$$

$$I_{Wm}^{u,v} = k_0^2\int\limits_{\Omega_1}\int\limits_{\Omega_2} (\mathbf{J}_u(\mathbf{r_1})\cdot\mathbf{J}_v^*(\mathbf{r_2}))\,\frac{\cos(k_0 r_{21})}{r_{21}}\mathrm{d}\Omega_1\mathrm{d}\Omega_2, \qquad (6)$$

$$I_{Wr}^{u,v} = \frac{k_0}{2}\int\limits_{\Omega_1}\int\limits_{\Omega_2}\left[k_0^2\left(\mathbf{J}_u(\mathbf{r_1})\cdot\mathbf{J}_v^*(\mathbf{r_2})\right)\right.$$
$$\left. - q_u(\mathbf{r_1})q_v^*(\mathbf{r_2})\right]\sin(k_0 r_{21})\mathrm{d}\Omega_1\mathrm{d}\Omega_2. \qquad (7)$$

Finally, the radiated power is determined as

$$P_r^{u,v} = \frac{1}{8\pi\omega_0\epsilon_0}\int\limits_{\Omega_1}\int\limits_{\Omega_2}\left[k_0^2\left(\mathbf{J}_u(\mathbf{r_1})\cdot\mathbf{J}_v^*(\mathbf{r_2})\right)\right.$$
$$\left. -q_u(\mathbf{r_1})q_v^*(\mathbf{r_2})\right]\frac{\sin(k_0 r_{21})}{r_{21}}\mathrm{d}\Omega_1\mathrm{d}\Omega_2. \qquad (8)$$

$W_e^{u,v}$, $W_m^{u,v}$ and $P_r^{u,v}$ define the energies and the total radiated power based on uth source (J_u or q_u) on domain Ω_1 and vth source (J_v or q_v) on domain Ω_2. In the $\mathcal{R}^3$ Euclidean space, the distance r_{21} is 2-norm distance $r_{21} = |\mathbf{r_2} - \mathbf{r_1}|$.

Note that for wavelength λ_0 the angular wavenumber $k_0 = 2\pi/\lambda_0$ and the charge density is defined as $q_u = \nabla\cdot J_u$. In most studied cases the domains Ω_1 and Ω_2 are equal ($\Omega = \Omega_1 = \Omega_2$), for $\Omega_1 \neq \Omega_2$ see [11].

III. MODAL Q FORMULATION

In order to obtain modal Q's, we have to introduce a proper modal method to obtain eigenmodes and eigenvalues. This method is, in our case, the Theory of Characteristic Modes.

Eigenmodes $\mathbf{j}_u$ and eigenvalues λ_u are physically vivid and valuable characteristics of electromagnetic operators such as the electric field integral equation (EFIE) [13], [14]. In the following text, spectral eigen-decomposition of the EFIE complex impedance matrix is performed in the frequency domain. The next section briefly summarizes the mathematical formulation of the EFIE as well as the TCM since it is crucial to know all the properties of relevant variables.

A. The Electric Field Integral Equation

The EFIE can be formulated by employing a boundary condition for the tangential incident ($\mathbf{E}^i$) and a scattered electric field on the perfect electric conductor (PEC)

$$\left[L(\mathbf{J}) - \mathbf{E}^i\right]_{\mathrm{tan}} = 0. \qquad (9)$$

The operator $L(\mathbf{J})$ is defined as

$$L(\mathbf{J}) = \mathrm{j}\omega\mathbf{A}(\mathbf{J}) + \nabla\phi(\mathbf{J}), \qquad (10)$$

where $\mathbf{A}(\mathbf{J})$ and $\phi(\mathbf{J})$ are vector and scalar potentials respectively [15]. Physically, $-L(\mathbf{J})$ gives the scattered

electric field intensity. Therefore, L has the characteristics of impedance

$$Z(\mathbf{J}) = [L(\mathbf{J})]_{\mathrm{tan}}. \qquad (11)$$

The solution of (11) can be treated directly

$$\mathbf{J}_{MoM} = \mathbf{Z}^{-1}\mathbf{E}^i \qquad (12)$$

as usually employed in the method of moments (MoM) [17] or by the superposition of the characteristic currents [12], [18]. This knowledge is important for our later expectations.[1]

In both cases, the impedance matrix and the (unknown) surface induced current density have to be expanded by appropriate basis functions (the most suitable are the well-known RWG basis functions $\mathbf{f}_s$ [19]); Galerkin's method is used.

The Q factor based on total current density from MoM has already been successfully calculated in [10] and [11] (MoM in Matlab with a thin-wire reduced kernel). However, to the knowledge of the authors, modal Q factors and stored energies have never been rigorously computed.

B. Theory of Characteristic Modes

The TCM evaluates the total surface current density as a sum of characteristic (eigen-) currents. They depend only on the shape and frequency, not on excitation. Details can be found in [12] and [20].

The impedance matrix $\mathbf{Z} = \mathbf{R} + \mathrm{j}\mathbf{X}$ is complex and symmetric (but not Hermitian), its parts $\mathbf{R}$ and $\mathbf{X}$ are real and symmetric. After a little manipulation we get the associated Euler's equation (a generalized eigenvalue problem)

$$\mathbf{Xj} = \lambda\mathbf{Rj}. \qquad (13)$$

A solution of (13) may easily be obtained using the `eig` routine in Matlab [21]. The square impedance matrix $\mathbf{Z}$ of order U (the number of inner edges) produces U eigen-pairs (λ_u, $\mathbf{j}_u$). Each eigenvector $\mathbf{j}_u$ together with the RWG functions forms the vector modal current density

$$\mathbf{J}(\mathbf{r}) = \sum_{u=1}^{U} j_u\mathbf{f}_u(\mathbf{r}), \qquad (14)$$

where the basis functions $\mathbf{f}_u$ are defined in [19].

The total current density can be expressed as a linear combination of these modal currents

$$\mathbf{J}_{tot} = \sum_{u=1}^{U}\alpha_u\mathbf{J}_u = \sum_{u=1}^{U}\frac{\langle\mathbf{j}_u, \mathbf{E}^i\rangle}{1 + \mathrm{j}\lambda_u}\mathbf{J}_u. \qquad (15)$$

The expansion coefficient α_u is obviously the modal amplitude. The result of $\langle\mathbf{j}_u, \mathbf{E}^i\rangle = \mathbf{j}_u^T\mathbf{E}^i$ is a scalar value called the modal excitation factor [20]. Remember that the $\mathbf{E}^i$ and $\mathbf{J}_{tot}$ have the same meaning in both MoM and TCM. Without the loss of generality, we consider only real feeding of $\mathbf{E}^i$ for the rest of the paper. It should be pointed out, that the sum (15) is in fact incomplete. There is certain portion of evanescent imaginary cur-

[1]To get more insight on the relationship between the direct MoM and the TCM see [16].

rent arising from the voltage-gap [22], contributing to the stored energies. This is reason why there are slight discrepancies between Q_M and Q_{Jtot} as will be seen later. Such residual current could be obtained as

$$\mathbf{J}_{res} = \mathbf{J}_{MoM} - \mathbf{J}_{tot} = \mathbf{Z}^{-1}\mathbf{E}^i - \sum_{u=1}^{U} \frac{\langle \mathbf{j}_u, \mathbf{E}^i \rangle}{1 + j\lambda_u} \mathbf{J}_u \qquad (16)$$

and its contribution included. Since its effect is not crucial, it is omitted here, however this issue is currently under study.

Thanks to the linearity of the divergence operator, the total charge density $q = \nabla \cdot \mathbf{J}$ is

$$q(\mathbf{r}) = \sum_{u=1}^{U} j_u \nabla \cdot \mathbf{f}_u(\mathbf{r}), \qquad (17)$$

and

$$\nabla \cdot \mathbf{f}_u(\mathbf{r}) = \begin{cases} \frac{l_u}{A_u^{\pm}} & \mathbf{r} \text{ in } \Omega_u^{\pm} \\ 0 & \text{otherwise} \end{cases} \qquad (18)$$

On the basis of (15)–(17) we have

$$\mathbf{q}_{tot} = \sum_{u=1}^{U} \alpha_u \mathbf{q}_u = \sum_{u=1}^{U} \frac{\langle \mathbf{j}_u, \mathbf{E}^i \rangle}{1 + j\lambda_u} \mathbf{q}_u. \qquad (19)$$

The modal decomposition (`eig` function) is time-consuming but can be parallelized.[2] Even thought the TCM forms the orthogonal set of modes, the eigencurrents are of yet indetermined amplitudes. This problem is handled by normalization to unit radiated power for each frequency of interest [12]

$$\langle \mathbf{J}_u^*, \mathbf{R}\mathbf{J}_u \rangle = 1 \text{ W} = P_r^{u,u}. \qquad (20)$$

C. Calculation of Modal Energies

Let us consider only (the first) two modes ($M = 2, u \in \{1, 2\}$) for simplicity and write out the current summation

$$\mathbf{J}_{tot} = \sum_{1,2} \alpha_u \mathbf{J}_u = \alpha_1 \mathbf{J}_1 + \alpha_2 \mathbf{J}_2. \qquad (21)$$

The total charge density is obtained in the same way. Because variables $\mathbf{f}_s$, $\mathbf{j}_u$ and $\mathbf{q}_u$ are real, both modal currents and charge densities are real. However, the coefficients $\alpha_u = \langle \mathbf{j}_u, \mathbf{E}^i \rangle / 1 + j\lambda_u$ are still complex and thus both the total current and charge densities are complex-valued.

If we take a look at (5)–(8), only parts $\mathbf{J}_u(d) \cdot \mathbf{J}_v^*(d)$ and $q_u(d)q_v^*(d)$ have to be worked out at a given frequency f_0 and on a triangularized shape Ω (or just a selected triangle T). Using (21)

$$\begin{aligned} \mathbf{J}_u(d) \cdot \mathbf{J}_v^*(d) &= \mathbf{J}_{tot}(d) \cdot \mathbf{J}_{tot}^*(d) \\ &= (\alpha_1 \mathbf{J}_1(d) + \alpha_2 \mathbf{J}_2(d))(\alpha_1^* \mathbf{J}_1(d) + \alpha_2^* \mathbf{J}_2(d)) \\ &= \underbrace{\alpha_1 \alpha_1^* \mathbf{J}_1 \cdot \mathbf{J}_1}_{\sim \text{INT11}} + \underbrace{(\alpha_1^* \alpha_2 + \alpha_1 \alpha_2^*) \mathbf{J}_1 \cdot \mathbf{J}_2}_{\sim \text{INT12, INT21}} \\ &\quad + \underbrace{\alpha_2 \alpha_2^* \mathbf{J}_2 \cdot \mathbf{J}_2}_{\sim \text{INT22}} \end{aligned} \qquad (22)$$

and analogously for the $q_u(d)q_v^*(d)$ part. Parts INT11/INT22 and INT12/INT21 are recognized as self and mutual interactions respectively. All discussed integrals may be divided in M^2 subintegrals (22) with corresponding modes u, v as the input data. For clarity, the "summation matrix" is introduced for electric/magnetic energy

$$\mathbf{W}_{e/m}^{M=2} = \begin{bmatrix} W_{e/m}^{11} & W_{e/m}^{12} \\ W_{e/m}^{21} & W_{e/m}^{22} \end{bmatrix} \sim \begin{bmatrix} \text{INT11} & \text{INT12} \\ \text{INT21} & \text{INT22} \end{bmatrix} \qquad (23)$$

The above procedure can be generalized to any number of modes (for proof see the Appendix). The total number of M modes form the energy matrices $W_{e/m}$ of $M \times M$ size. Then the radiation Q is expressed by a novel relation

$$Q_M = 2\omega_0 \frac{\max \left\{ \sum_u^M \sum_v^M \beta_{u,v} W_e^{u,v}, \sum_u^M \sum_v^M \beta_{u,v} W_m^{u,v} \right\}}{\sum_u^M \sum_v^M \beta_{u,v} P_r^{u,v}}, \qquad (24)$$

where the coupling matrix β is written as

$$\beta_{u,v} = \frac{\langle \mathbf{j}_u, \mathbf{E}^i \rangle \langle \mathbf{j}_v, \mathbf{E}^i \rangle (1 + \lambda_u \lambda_v)}{(1 + \lambda_u^2)(1 + \lambda_v^2)}. \qquad (25)$$

Using the Hadamard product $(A \circ B)_{u,v} = (A)_{u,v}(B)_{u,v}$ [23]

$$Q_M = 2\omega_0 \frac{\max \left\{ \sum_{u,v} (\boldsymbol{\beta} \circ \mathbf{W}_e)_{uv}, \sum_{u,v} (\boldsymbol{\beta} \circ \mathbf{W}_m)_{uv} \right\}}{\sum_{u,v} (\boldsymbol{\beta} \circ \mathbf{P}_r)_{uv}}. \qquad (26)$$

Modal energies $W_e^{u,v}$ and $W_m^{u,v}$ respect (3) and (4) with input current and charge densities (14) and (17) respectively. $\mathbf{W}_{e/m}$ and $\boldsymbol{\beta}$ are in matrix form (23). At a given frequency, eigenvectors $\mathbf{j}_{u,v}$, eigenvalues $\lambda_{u,v}$ and stored modal energies $W_{e/m}^{u,v}$ are known. Therefore, the total Q_M factor can be tuned by just a single parameter—the actual feeding $\mathbf{E}^i$. In Section V we will verify that (24) is close to the total Q and is suitable for use in antenna design.[3] Both modal (3), (4) and total (23) energies give important additional information about the radiating structure. It is worth noting that the total Q factor can only be calculated from the modal stored energies and powers—direct superposition of modal Q factors is impossible.

IV. SOFTWARE IMPLEMENTATION

The EFIE core is based on the RWG elements [24]. Thus, proper discretization has to be employed. The Matlab PDE toolbox usually creates mesh of poor quality (particularly for complex shapes like fractals), better results are obtained by the Comsol Multiphysics mesh generator. In order to control meshing, the authors work on an in-house mesh generator that employs the `distmesh` code from MIT [25]. In this paper we assume that the analysed geometry Ω is properly triangularized into T triangles with U inner edges. Note that the quality and number of triangles are crucial for the resulting convergence of the solution.

---

[2]This has been done via the Matlab Distributed Computing toolbox gaining a speed-up of about 9 for 12 nodes.

[3]For $M \to \infty$, the Q_∞ in (24) is simply equal to total Q. In practice, however, it is sufficient to sum only finite (low) numbers of modes $M \approx 5$.
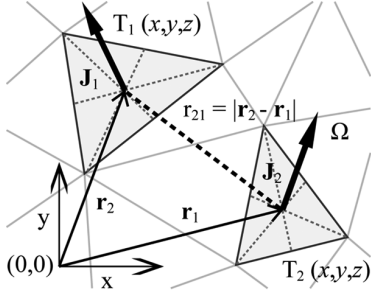
Fig. 1. Distance between non-overlapping current elements.

MoM solutions of thin-strip structures are usually assumed to be fed by the delta-gap [15]. Some planar structures are fed by the incident plane wave—usually only the x- or y-component $\mathbf{E}^i = [E_x, E_y, E_z]$ is used, [24]. The respective eigenproblem is solved in Matlab and all modes are sorted (tracked) and represented in terms of the characteristic angles [26]

$$\delta_u = 180 - \arctan(\lambda_u). \qquad (27)$$

The characteristic angles are continuous through the values of 90-270, resonance of the uth mode occurs when $\delta_u = 180$. An illustrating example is shown in Section V.

A. Numerical Evaluation of $W_{e,m}$ and P_r—Distant Elements

The key expressions (5)–(8) consist of double surface integrals over a given planar structure Ω. In our case, Ω is discretized using the Delaunay triangulation, Fig. 1. Hence the integration is now performed via the compact set of triangles T.

The modal current matrices $\mathbf{J}_{u/v}$ are calculated from eigenvectors and the RWG basis function via (14). The order of $\mathbf{j}_{u/v}$ is $1 \times U$, but the order of the modal current $\mathbf{J}_{u/v}$ is $3 \times T$. Similarly, the modal charge distributions are calculated from (17) and each matrix $\mathbf{q}_{u/v}$ is of order $1 \times T$. Thus, one current vector $[J_x, J_y, J_z]$ and charge density q are assigned to each triangle. These values are considered constant throughout the triangle area and are assumed to be located at the centre of the triangles [27]. It will be shown later that this centroid approximation is accurate enough. However, it could fail e.g. for patch antennas at very small heights above the ground plane.

B. Numerical Evaluation of $W_{e,m}$—Overlapping Elements

As one can see, there are singularities in (5) and (6) for overlapping triangles $(T_1 = T_2)$. The so-called self-coupling term [28] plays a major role in Q factor calculation and therefore it should be treated carefully. We are looking for a fast and sufficiently accurate solution to the following problem:

$$I_1(T_1 = T_2) = \int\limits_{T_1} \int\limits_{T_2} \frac{\cos(k_0 r_{21})}{r_{21}} \mathrm{d}t_1 \mathrm{d}t_2, \qquad (28)$$

where $r_{21} = \sqrt{(x_2 - x_1)^2 + (y_2 - y_1)^2 + (z_2 - z_1)^2}$. The (28) is expanded in a Maclaurin series and since $k_0 R_{21} \to 0$ (R_{21} is the longest side of the triangle T_1) is satisfied, one can only use its first term. Then the cosine function $\cos(k_0 r_{21})$ from (28) reduces to the static singular part $1/r_{21}$. There is still a problem with the triangular region of integration.

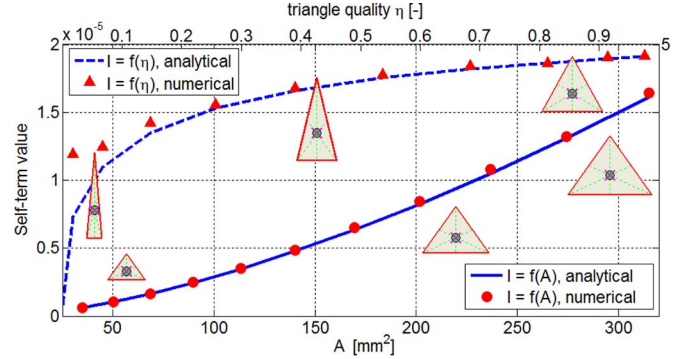| edges	1st mode				2nd mode	
	P_r [W]	Q_1	e_1 [%]	t [s]	Q_2	e_2 [%]
42	1.0041	0.738	87.23	0.015	–	–
180	1.0007	0.804	95.04	0.016	0.666	77.99
412	1.0002	0.814	96.25	0.031	0.789	92.39
926	0.9999	0.853	100.83	0.125	0.830	97.19
1691	0.9998	0.854	100.95	0.390	0.825	96.60
4704	0.9997	0.846	100	2.621	0.854	100

Fig. 2. Self-term values depending on the quality and area of the triangle.

The above issue was solved e.g. in [28] and the result was simplified in accordance with [29]

$$I_2 = -\frac{4}{3}A^2 \left(\frac{\ln\left(1 - \frac{2|\mathbf{h}_{12}|}{O}\right)}{|\mathbf{h}_{12}|} + \frac{\ln\left(1 - \frac{2|\mathbf{h}_{13}|}{O}\right)}{|\mathbf{h}_{13}|} + \frac{\ln\left(1 - \frac{2|\mathbf{h}_{23}|}{O}\right)}{|\mathbf{h}_{23}|} \right), \qquad (29)$$

where $|\mathbf{h}_{12/13/23}|$ denote the length of the edges of the triangle and O is its perimeter. The computational cost of evaluating (29) is mainly determined by the ln functions (see fifth column in Table I).

Fig. 2 shows the behaviour of (29) while varying the triangle area and the triangle quality which is defined as

$$\eta = \frac{4\sqrt{3}A}{|\mathbf{P}_1 - \mathbf{P}_2|^2 + |\mathbf{P}_1 - \mathbf{P}_3|^2 + |\mathbf{P}_2 - \mathbf{P}_3|^2}. \qquad (30)$$

The coefficient η is between 0 (three points on a line) and 1 (equilateral triangle). When varying the triangle area, quality is fixed (at value $\eta = 0.98$, solid line at Fig. 2) and when varying the triangle quality, area is fixed (dashed line at Fig. 2).

Finally note that the term $\sin(k_0 r_{21})/r_{21}$ in (8) is not singular and changes negligible within the triangle

$$\lim_{r_{21} \to 0} \frac{\sin(k_0 r_{21})}{r_{21}} = k_0 \lim_{k_0 r_{21} \to 0} \frac{\sin(k_0 r_{21})}{k_0 r_{21}} = k_0 \qquad (31)$$

C. Convergence Analysis

It is very important that the algorithm is convergent with an increasing number of RWG basis functions (the parameter U). To verify this assumption, we consider a 30 × 20 cm rectangular plate in free space. This plate is discretized with a different number of triangles and analyzed using the TCM solver. Then,
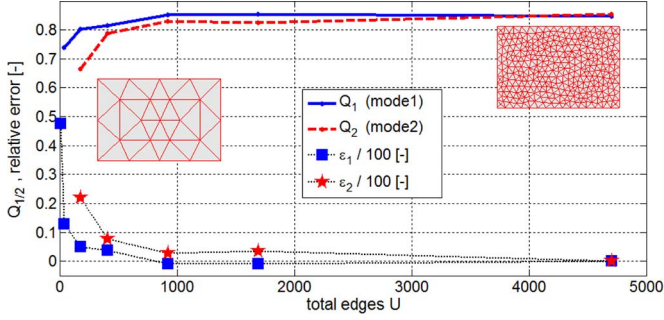
Fig. 3. Algorithm convergence, rect. plate 30 × 20 cm.

Fig. 4. The original data from the TCM (left) and the sorted ones (right), rec. plate 30 × 20 cm (634 triangles, 926 edges).

modal radiated power and Q factors are calculated for the 1st and 2nd modes, see Table I.

In terms of convergence, (8) is very interesting since from (20) it is observed that the modal radiated power should be equal to one (in case of 1st mode $u = v = 1$). Table I confirms that the modal radiated power P_r is very close to 1 W.

It can therefore be assumed that the numerical integration of radiated power (8) as well as the stored energies (3) and (4) are performed correctly. Singularity treatment can be illustrated at Fig. 3, which shows the convergence of modal Q factors for the 1st and 2nd modes of the rectangular plate. Note, that the inaccurate Q results for low values of U (typically fewer than 150 edges) are caused by a poorly conditioned TCM task. In the case of 42 edges the resonant frequency of the second mode was not found.

Given that energies $W_e^{u,v}$ and $W_m^{u,v}$ are very small (ranging in the order of $10^{-7} \div 10^{-9}$ relative to the unit radiated power), we can conclude that the convergence is sufficient.

Run-time complexity: The complexity of the TCM solution for F frequency samples is $\mathcal{O}(FU^3)$. Considering just one mode at a single frequency, the modal energy computation has a quadratic time complexity $\mathcal{O}(T^2)$ (see the 5th column in Table I). Finally, the complexity of (24) is $\mathcal{O}(Q_M) \propto \mathcal{O}(M^2T^2)$. Because it is sufficient to calculate only half of all the energies $W_e^{u,v}$ and $W_m^{u,v}$ (see Appendix), the time-complexity is $\mathcal{O}(Q_M) \propto \mathcal{O}((M^2/2)T^2)$. And since in practice $M \ll U$, the total calculation time is strongly dominated by the eigen-decomposition, see Section V-D2. Fortunately, in the frequency domain both (13) and (24) can be parallelized (at most F nodes may be employed).

D. Tracking of Eigenvalues and Eigenvectors

The spectral decomposition of the moment impedance matrix $\mathbf{Z}$ doesn't always produce well ordered eigenmodes (see Fig. 4 left). This issue is particularly caused by finite numerical accuracy and slight asymmetry of the frequency-dependent matrix (although the MoM code is based on the Galerkin testing procedure, the Z-matrix is not purely symmetrical). At specific frequencies, the decomposition issue might be ill-posed and non-uniquely defined as well.

Proper manipulation and tracking of the modes is the key to preventing physically different current distributions along the frequency samples. Many matrix preconditioners could be used but the resulting modes still need tracking. There are many issues that have to be considered and therefore a specific heuristic
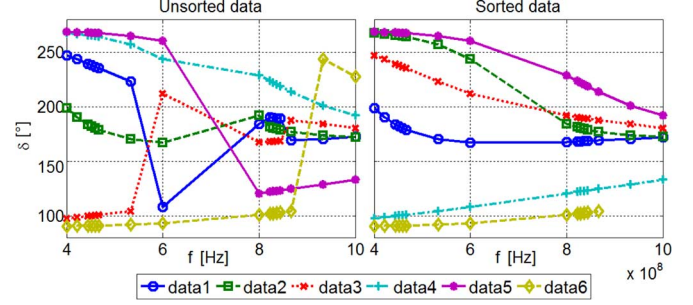
method was coded and implemented. Detailed description is beyond the scope of this paper although further information can be found in [30].

Another problem is caused by slight asymmetry of the TCM solution (currents are not ideally orthogonal to each other) and the fact that the current $\mathbf{J}_{u/v}$ can be computed with random sign. To explain this matter, we extend (13) to a formally correct form $C\mathbf{X}\mathbf{j} = C\lambda\mathbf{R}\mathbf{j}$. While the magnitude of the constant C can be removed by normalization to unit radiated power $\widehat{\mathbf{j}} = \mathbf{j}/\sqrt{\langle \mathbf{j}, \mathbf{R}\mathbf{j}\rangle}$, the sign of C remains unchanged.[4]

Fig. 4 shows that the frequency samples aren't spaced equidistantly. This is because that an adaptable frequency solver (AFS) is used in our tool. The AFS starts with an initial set of samples (specified by the user) and then dynamically adds additional samples to the locations with large changes in eigenvalues. This technique significantly saves computational time and helps the tracking of modes.

V. APPLICATION: NUMERICAL RESULTS

In this section we demonstrate our efforts on some selected problems. To validate the above mentioned approach, several Q estimates are compared.

The radiation Q factor may be estimated from the input impedance $\mathbf{Z}$ variation around the resonant frequency f_0 [2]

$$Q_Z = \omega_0 \frac{\left| \frac{\partial Z(\omega)}{\partial \omega} \right|}{2R(\omega_0)}. \tag{32}$$

The above equation could be converted to the modal form Q_{Zu}. Let us expand both the numerator and the denominator by current $|I|^2/2$ and suppose that Ω is PEC

$$Q_Z = \omega_0 \frac{\left| \frac{\partial R(\omega)}{\partial \omega} + j\frac{\partial X(\omega)}{\partial \omega} \right| \frac{|I|^2}{2}}{2R(\omega)\frac{|I|^2}{2}}$$

$$= \frac{\omega_0 \left| \frac{\partial (P_r)}{\partial \omega} + j\frac{\partial (2\omega(W_m - W_e))}{\partial \omega} \right|}{2P_r} \tag{33}$$

Since from (20) $P_r = 1$ W, implying that $\partial(P_r)/\partial\omega = 0$, then

$$Q_{Zu} = \frac{\omega_0}{2} \left| \frac{\partial (2\omega(W_m^u(\omega) - W_e^u(\omega)))}{\partial \omega} \right| \tag{34}$$

[4]This causes problems on adjacent frequencies. For example the current orientation at frequency F is $\{J_u, J_v\} \sim \{+, +\}$ and at freq. $F + 1$ is $\{J_u, J_v\} \sim \{+, -\}$. Then, due to the slight non-orthogonality, the results at F and $F + 1$ are significantly different.

TABLE II
COMPARISON OF ALL DEFINED Q THAT CONSIDER FEEDING

	Q_Z	Q_{MoM}	Q_{Jtot}	Q_M
Equation	(32)	(11)	(15)	(37)
Source	Z_{in}	$\mathbf{J}_{MoM}, \mathbf{q}_{MoM}$	$\mathbf{J}_{tot}, \mathbf{q}_{tot}$	$\boldsymbol{\beta}, \mathbf{W}_{e/m}$
Reference	[2]	[10]	$\times$	$\times$
Based on solver	MoM	MoM	TCM	TCM
Comp. speed	+++	++	+	+++
Information	+	++	++	+++

TABLE III
COMPARISON OF MODAL APPROACHES TO CALCULATION OF Q

	Q_n	$Q_{u,v}$	$\mathbf{W}_{e/m}$
Equation	(35)	(1)	(3), (4)
Source	λ_n	$\mathbf{W}_{e/m}$	$\mathbf{J}_u, \mathbf{q}_u$
Reference	[31]	$\times$	[10]
Based on solver	TCM	TCM	$\times$
Comp. speed	++	+++	+
Information	+	+++	++

The second modal-approach relation is based on the Rayleigh quotient formula for eigenvalue λ_n, [31]

$$Q_n = \frac{\omega_0}{2} \left| \frac{\partial \lambda_n(\omega)}{\partial \omega} \right|, \qquad (35)$$

where $\partial \lambda_n / \partial \omega$ is the slope of the nth eigenvalue. Expressions (34) and (35) are equal, provided that

$$2\omega \left(W_m^u(\omega) - W_e^u(\omega) \right) = \lambda_u(\omega). \qquad (36)$$

It can be proven that at resonance $Q_n = Q_{Zu}$. The above derived (24) can be formally simplified by using the Frobenius product, [23]. Because the Frobenius product is an inner product of the vector space, we use the same notation as in (15) or (20)

$$Q_M = 2\omega_0 \frac{\max \left\{ \langle \boldsymbol{\beta}, \mathbf{W}_e \rangle, \langle \boldsymbol{\beta}, \mathbf{W}_m \rangle \right\}}{\langle \boldsymbol{\beta}, \mathbf{P}_r \rangle}. \qquad (37)$$

It has to be noted that (37) is the total Q factor calculated from M selected modes. However, if we consider only one mode u (without any feeding, $\beta_u = 1$), the corresponding Q factor will be referred to as the Q_u factor.

In many cases it isn't necessary to consider the whole matrix $\boldsymbol{\beta}$ because only the diagonal terms $u = v$ are relevant (the others are typically in the order of 10^{-20}, see Section V-B). We denote the diagonal terms as β_u.

Finally, for the comparison of Q_M, we introduce two more radiation factors Q_{MoM} and Q_{Jtot}. Both are also calculated using (3)–(8). The input current distribution $\mathbf{J}_{MoM}$ of factor Q_{MoM} is obtained directly from MoM, the total current $\mathbf{J}_{tot}$ of factor Q_{Jtot} is calculated by (15). See Table II and Table III for comparison of all defined radiation factors.

All the following examples are chosen in order to clarify the presented results. At first, we verify the modal method (RWG, TCM), then we calculate (32)–(37) and compare them with each other.

A. The Thin-Strip Dipole

The first antenna is a dipole in a free space. The length $2L$ is 300 mm and the width d is 2 mm. The dipole was discretized into 432 triangles (534 inner edges) and fed by a voltage gap
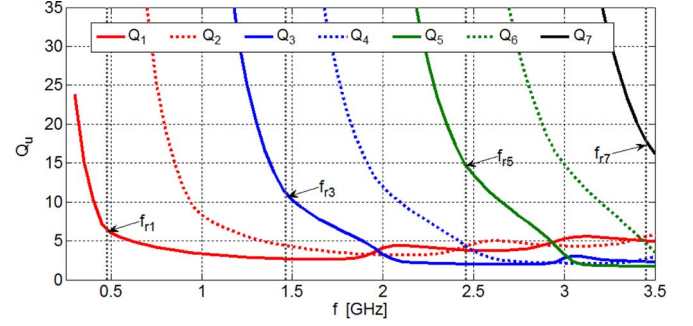

Fig. 5. The first seven modal Q_u factors of the 300×2 mm dipole.

TABLE IV
MODAL Q FACTORS IN RESONANCE AND THE β_u FACTORS FOR DIPOLE

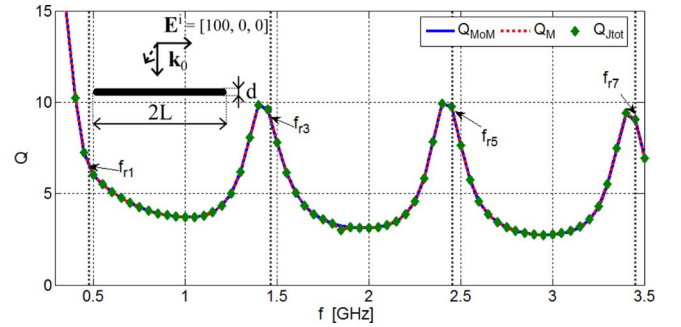| u	f_r [MHz]	Q_n	Q_{Zu}	Q_u	$\beta_{u(1/2)}$	$\beta_{u(1/4)}$
1	475.9	6.78	6.20	6.62	93.29	50.03
2	969.0	9.15	8.28	8.93	$8 \cdot 10^{-23}$	95.31
3	1463.7	11.16	10.02	11.09	84.72	40.04
4	1959.3	12.93	11.53	13.00	$3 \cdot 10^{-24}$	0.20
5	2455.5	14.52	12.88	14.91	78.76	44.50
6	2952.4	16.00	14.09	16.43	$2 \cdot 10^{-22}$	76.44
7	3449.9	22.11	19.41	19.37	70.26	33.23

Fig. 6. Q_{MoM}, Q_M and Q_{Jtot} for the dipole 300×2 mm fed by an incident plane wave.

[15]. This structure is analyzed over a large frequency band (including the small antenna regime).

Let us look first at the modal Q_u factors that form the total Q_M. The first seven modal Q_u factors ($u \in \{1, \ldots, 7\}$) are depicted at Fig. 5. It is worth mentioning that all modes cyclically intertwine with each other in the lower right corner of Fig. 5. Table IV shows all modal Q factors compared numerically at the resonant frequency of each mode. Modal Q approximations (34), (35) and the exact Q_u factor agree quite well.

Further analysis assumes that the dipole is being excited. We consider an incident plane wave as well as two different feed edge positions.

At first, the total Q_M with incident plane wave feeding is shown at Fig. 6. The incident wave is polarized in the x-direction ($\mathbf{E}^i = [100, 0, 0]$). In this case, the agreement of Q_{MoM}, Q_M and Q_{Jtot} is excellent.

1) Central Feeding: The dipole is fed by a voltage gap ($E^i = 100$ V) located at the middle edge. The modal factors Q_u are not changed as they describe the intrinsic behaviour of the radiator. Due to symmetry, only odd modes are excited (see column $\beta_{u(1/2)}$ in Table IV).
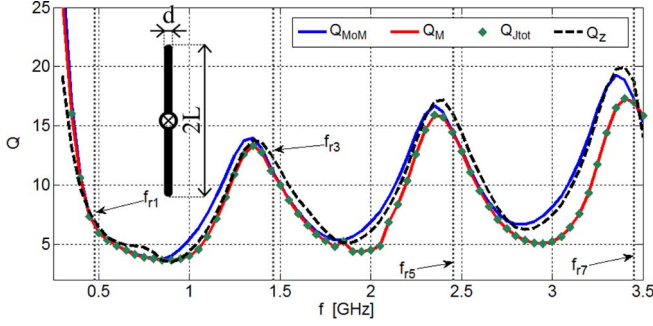
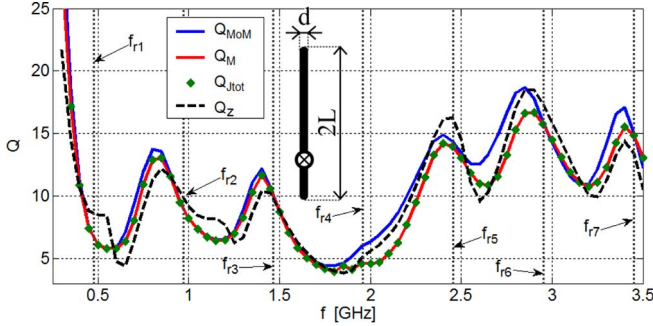Fig. 7. Q_{MoM}, Q_M, Q_{Jtot} and Q_Z of the dipole 300×2 mm, feeding is placed in the middle of the dipole.

Fig. 8. Q_{MoM}, Q_M, Q_{Jtot} and Q_Z of the dipole 300×2 mm, feeding is placed at one quarter of the dipole length.

Fig. 9. Q_{MoM}, Q_M, Q_{Jtot} and Q_Z for in-phase fed dipoles of distance d.

Fig. 10. The first four modal Q_u factors (two dipoles of distance $d = 0.18\lambda$).

TABLE V
MODAL Q FACTORS IN RESONANCE FOR TWO COUPLED THIN-STRIP DIPOLES
OF DISTANCE $d = 0.18\lambda$ (MINIMAL TOTAL Q)

u	f_r [MHz]	Q_n	Q_{Zu}	Q_u
1	1386.5	31.40	27.21	26.74
2	1437.2	3.39	3.12	**3.01**
3	2816.3	15.52	13.98	15.17
4	2980.2	5.72	5.07	5.09

This explains why total Q factors at Fig. 7 are affected only by odd modal Q_u factors (see solid lines at Fig. 5). Comparison between Fig. 6 and Fig. 7 shows that the voltage gap case converges relatively poorly because of issues mentioned at Section III-B.

The total Q factor is an oscillating function with an absolute minimum of $f/f_{r1} \doteq 1.76$, see Fig. 7. It can be seen, that the agreement of the Q_{MoM} with the Q_Z approximations (directly derived from impedance matrix **Z**) is quite good. Slight differences between Q_M and Q_{Jtot} at higher frequencies are also (except for the voltage gap issue) addressed by the fact that Q_M is calculated only for the first few modes M, which may no longer be effective at higher frequencies.

2) Feeding at 1/4 of the Dipole Length: Now the dipole is fed at the 1/4 of its length, more modes can be now excited and accordingly, the coefficients β_u changed significantly (see column $\beta_{u(1/4)}$ in Table IV). Hence the total Q factors at Fig. 8 are notably different as well—compare to Fig. 7. With the exception of the fourth mode (which cannot be excited), all modes somehow contribute to the total Q_M.

This example shows how the modal approach is effective and illuminating. The eigenproblem is calculated only once, after that we consider only the arrangement of the excitation.

B. The Mutually Coupled Dipoles—In-Phase Currents

The second example studies the Q factor of two side-by-side coupled dipoles. Both are 100 mm long and 1 mm wide, spaced by the distance d and fed in the middle of the antenna(s) with the same amplitude and phase ($E^i = 100$ V, $\mathbf{J}_1 = \mathbf{J}_2$). Dipoles
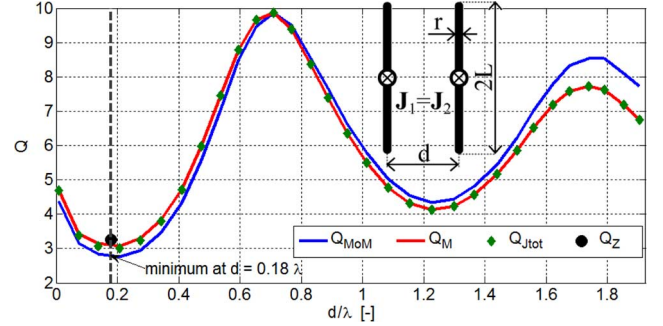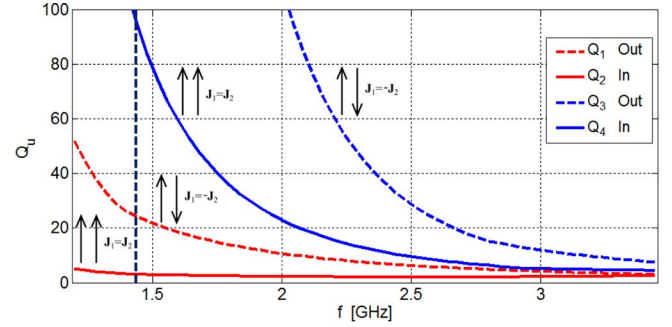
were discretized into 576 triangles (718 inner edges). This scenario is equivalent to a single horizontal dipole lying $d/2$ above a perfect magnetic infinite plane (PMC).

The total Q_M factor was calculated as a function of distance d. Comparison with other total Q factors is depicted at Fig. 9. Again, the total Q_M is an oscillating function with an absolute minimum of $d = 0.18\lambda$. While the case of out-of-phase currents was analytically verified in [11] ($d(\min(Q)) = 0.716\lambda$), for in-phase currents a similar study is more complicated.

Nevertheless, this behaviour can be easily explained by the TCM. Resonant frequencies and modal quality factors are displayed in Table V, Fig. 10 shows the first four modal Q_u factors ($u \in \{1, 2, 3, 4\}$); current orientation is schematically depicted as well. Table V shows that the in-phase modes have significantly lower Q_u than the out-of-phase modes.

Obviously, the total in-phase current is formed by the dominant in-phase mode at a given frequency (which is the frequency of the second mode with $f_{r2} = 1437.2$ MHz and $Q_u = 3.01$). Let us consider summation of four modes at frequency $f = f_{r2}$ and for distance $d = 0.18\lambda$. Then we obtain the values in Table VI. For Q_M calculation at this point, we can omit all coefficients and energies of an order less than 10^{-10}. In this case that is all except the second mode ($u = v = 2$), see Table VI).

TABLE VI
SUMMATION DATA AT RESONANCE FOR 2ND MODE ($f_{r2} = 1437.2$ MHz, IN-PHASE CURRENT) OF TWO COUPLED THIN-STRIP DIPOLES WITH DISTANCE $d = 0.18\lambda$ (MINIMAL TOTAL Q)

u	$\beta_{u,u}$ [-]	λ_u [-]	$2\omega(W_m^u - W_e^u)$	Q_u
1	$7 \cdot 10^{-24}$	1.72	1.94	24.42
2	**156**	**0.01**	**0.04**	**3.01**
3	$5 \cdot 10^{-29}$	-759.38	-680.53	902.10
4	$2 \cdot 10^{-27}$	-80.54	-72.64	95.48

Also all products of $\beta_{u,v} W_{e/m}^{u,v}$ for $u \neq v$ are negligible. As a result, only the second mode contributes to the total Q

$$Q_M = 2\omega_0 \frac{\max \left\{ \beta_2 W_e^{2,2}, \beta_2 W_m^{2,2} \right\}}{\beta_2 P_r^{2,2}}. \tag{38}$$

Since $P_r^{2,2} \doteq 1$, we simplify (38) by extracting β_2

$$Q_M = 2(2\pi f_{r2}) \max \left\{ W_e^{2,2}, W_m^{2,2} \right\}$$
$$= 4\pi 1.437 \cdot 10^9 \max\{1.642 \cdot 10^{-10}, 1.663 \cdot 10^{-10}\}$$
$$= 3.01$$

It is seen that the minimal $Q_M = 3.01$ is directly equal to the modal Q_u of the second mode.

Note that the above described behaviour is also valid for the folded dipole with sufficient conductor coupling and a separation distance of $d \ll 0.05\lambda$.

C. The Bowtie Antenna

The next antenna under study is a bowtie in a free space. Its length L is 100 mm, width d is 60 mm and gap width t is 4 mm, see Fig. 13. The structure is discretized into 309 triangles with 436 inner edges (these values are doubled in the case of an infinite ground plane as described later). Two feeding scenarios have been considered—incident plane waves with polarizations $\mathbf{E}_1^i = [100, 0, 0]$ and $\mathbf{E}_2^i = [100, 100, 0]$.

The first step is the modal analysis of the bowtie without a ground plane. Characteristic angles are shown at Fig. 11 (solid lines), Fig. 12 depicts schematically the main current paths of these modes. For clarity we show only the first five modes, but in fact we analyze the first ten significant modes at a given frequency range. Nonetheless the results may be inaccurate at the end of the frequency spectrum (about $3.5 \div 4$ GHz).

Polarization of the incident plane wave dramatically affects the total sum for Q—Fig. 13. Total Q factors are the same for both polarizations up to a frequency of about 2.3 GHz. For higher frequencies, results start to strongly depend on the excitation of modes 2–10.

An interesting study is presented at Fig. 14, only $\mathbf{E}_1^i$ polarization is assumed. All the first ten modes are divided into four groups (see Fig. 14 left), while each group contains similar modes (regarding current distributions). Fig. 14 shows the effects on the total Q_M depending on which groups are summed up. It is clearly seen that the inductive (non-radiating, group D at Fig. 14 left) modes significantly affect the behaviour of the antenna (compare sum $A + B + C$ and $A + B + C + D$ at Fig. 14 right).

Then the bowtie is placed above an infinite ground plane at a height of h. Changes in eigen-angles are depicted at
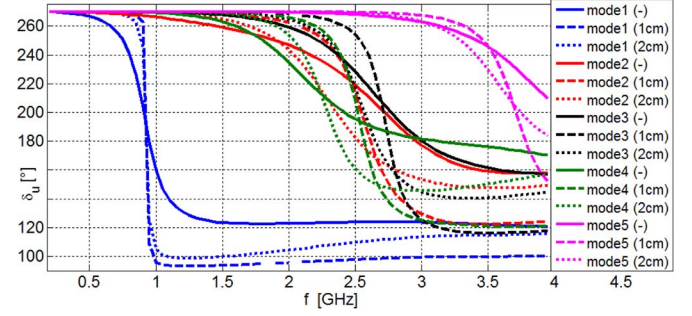

Fig. 11. The first five modes represented by the eigen-angles δ_u as a function of frequency, the bowtie antenna (solid line: no ground plane; dashed lines: infinite ground planes of height 1 cm and 2 cm, respectively).
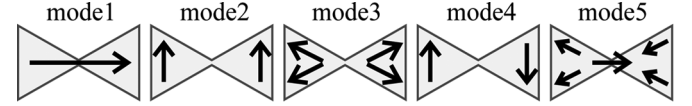

Fig. 12. Schematic depiction of the first five modes of the bowtie antenna.
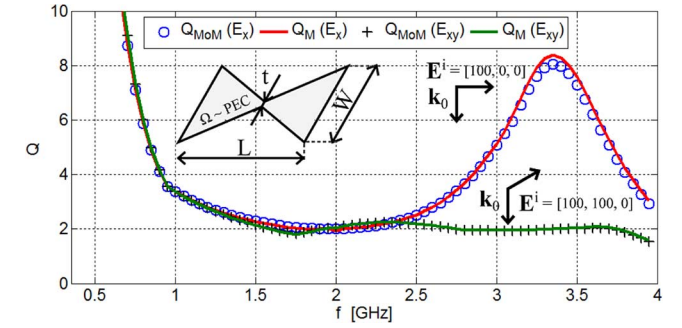

Fig. 13. Q_{MoM} and Q_M of the bowtie (two incident plane wave polarizations are considered).
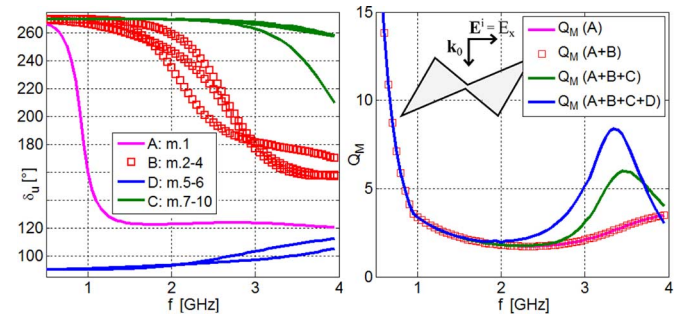

Fig. 14. The first ten modes of bowtie with associated four scenarios of Q_M factors (E_x polarization).

Fig. 11. With increasing height above the ground, the slope of eigen-angles decrease. Because of a minimum (and more or less constant) resonant frequency, only the dominant mode TM_{01} (without any feeding) will be studied. Using the image theory [15], the radiator in the $x - y$ plane placed h above the infinite electric ground plane is modeled as two bowties separated by the distance $2h$, see Fig. 15. In the TCM analyzer, proper out-of-phase mode is selected and analysed.

The modal factors Q_u and Q_n of the first mode are depicted at Fig. 16. These were obtained at resonance ($\delta_u = 0$) as a func-
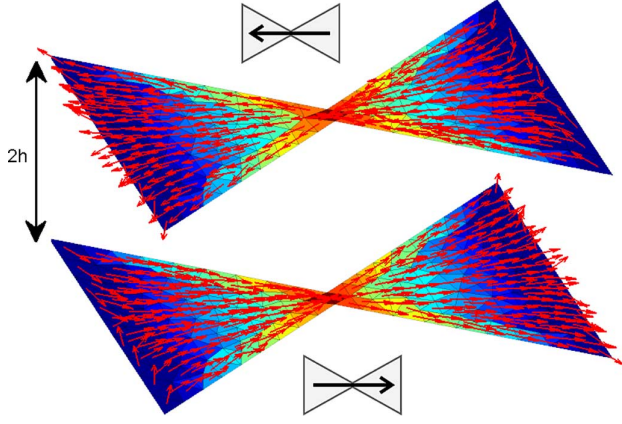
Fig. 15. Bowtie above infinite ground plane $h = 5$ mm, dominant mode TM_{01} shown.
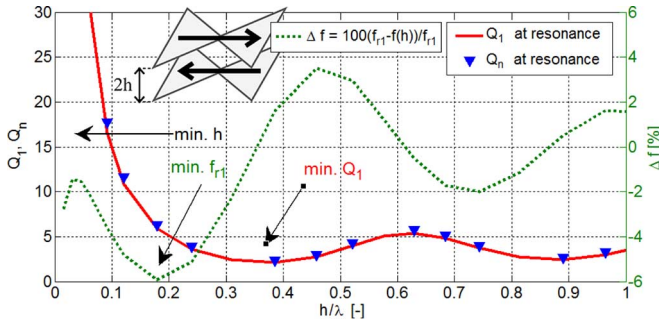

Fig. 16. The modal radiation Q_u and the resonant frequency for dominant mode of bowtie antenna as a function of height h.
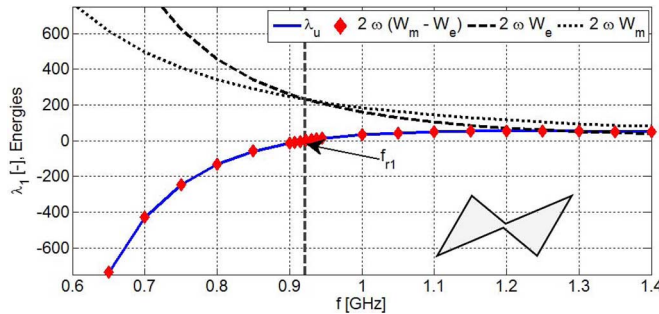

Fig. 17. The eigenvalues, electric and magnetic stored energies of the first mode at height 5 mm, bowtie.

tion of height h. For larger values of h the Q_u factor becomes smaller. The second curve at Fig. 16 (green dashed line) represents changes in the resonance frequency of the first mode, calculated as

$$\Delta f_\% = 100 \frac{f_{r1}(\infty) - f_{r1}(h)}{f_{r1}(\infty)} \qquad (39)$$

and displayed in [\%]. This allows us to locate zones with minimum values of h and Q_u and to find a compromise between them for a specific application. For comparison, the reactive energies of the 1st mode for height $h = 5$ mm $(f_{1r} = 927 \text{ MHz})$ are plotted at Fig. 17. It is obvious that resonance occurs when the stored energies are equal and so the eigenvalue $\lambda_1 = 0$, (36).
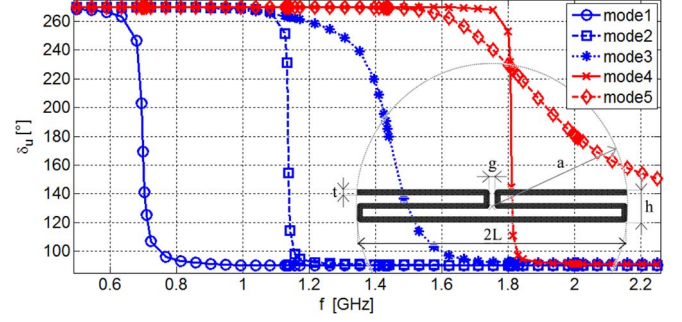

Fig. 18. The first five characteristic angles of meander folded dipole.

TABLE VII
MODAL Q FACTORS IN RESONANCE FOR MEANDER FOLDED DIPOLE (THE FIRST FIVE MODES ARE CONSIDERED)

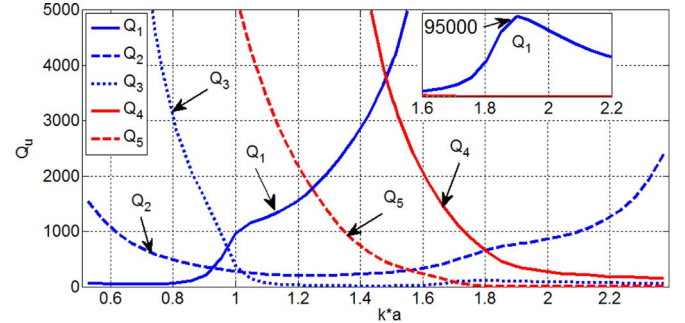| u	f_r [MHz]	ka	Q_n	Q_u
1	697.8	0.736	43.34	43.54
2	1136.5	1.199	196.67	195.83
3	1442.2	1.521	13.76	13.82
4	1809.2	1.908	357.40	355.52
5	2005.1	2.115	3.45	3.41

Fig. 19. The modal Q_u of the first five modes of meander folded dipole.

D. The Meander Folded Dipole

The last example is an electrically small meander folded dipole. Length $2L$ is 100 mm, overall width h is 12 mm (so enclosing a sphere of radius $a = \sqrt{L^2 + (h/2)^2} = 50.35$ mm), the width of strip t is 2 mm and the gap width g is also 2 mm. The dipole is discretized into 736 triangles with 929 inner edges. All the outer corners are bent with radius 1 mm and refined—see the lower right corner of Fig. 18. The frequency range for analysis is chosen from 0.5 GHz $(ka = 0.527)$ to 2.25 GHz $(ka = 2.373)$.

Modal analysis is performed with an adaptable frequency solver. The initial frequency step is set to 50 MHz (36 samples) with two additional iterations (60 samples are obtained at the end of calculation). Eigen-numbers are successfully sorted and converted to the eigenangles, see Fig. 18. There are five modes that are dominant in the selected frequency range.

The modal radiation factors Q_n (only at resonance) and Q_u were calculated for each mode, see Table VII and Fig. 19. The difference between Q_n and Q_u is caused primarily by numerical evaluation of derivation in (35), so the calculation of Q_n gets more inaccurate with higher values of Q. Also in this case the AFS solver is very useful. Note that the first mode is purely inductive at mid-range frequencies, thus the Q_1 rises very fast
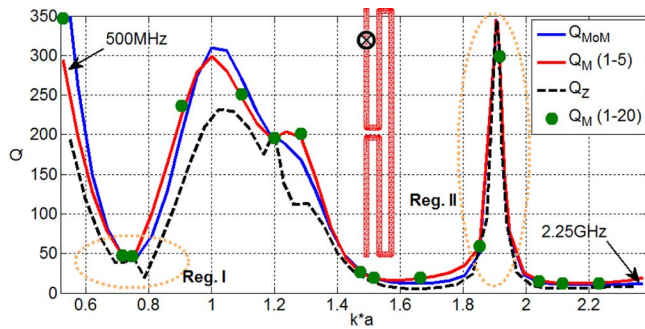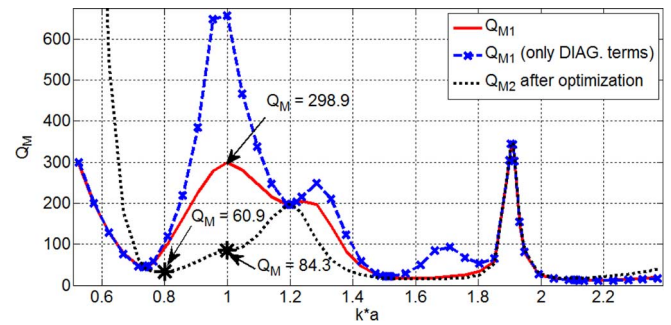
Fig. 20. Q_{MoM}, Q_M and Q_Z of meander folded dipole.

Fig. 21. Total Q_M calculation based on various number of modes (numbers in the legend characterize what modes have been summarized).

Fig. 22. Comparison between full Q_M and Q_M based only on diagonal terms in matrix $\boldsymbol{\beta}$, minimalized Q_M is displayed as an asterisk.

Fig. 23. $\boldsymbol{\beta}$ matrix for two feeding scenarios: the original feeding ($Q_M = 298.9$ at $ka = 1$) and the optimized feeding ($Q_M = 84.3$ at the same ka), first five modes are considered.

(reaching a value of 95000). A detailed description of the modal currents is beyond the scope of this paper.

1) Total Q_M Calculation: To obtain the total Q (both Q_M, Q_Z and Q_{MoM}), feeding has to be incorporated. For this purpose a voltage gap generator ($E^i = 100$ V) was placed at the inner edge of no. 39, highlighted at Fig. 20. Then the total Q factors are calculated and are shown at Fig. 20. Some observations are listed as follows.

- The course of Q_M is smooth and more or less equal with Q_{MoM}. On the other hand, Q_Z doesn't match very well, especially in locations distant from the modal (natural) resonances, [2].
- Q_M (1–5) for the first five modes is close to Q_M (1–20) for the first 20 modes (Q_M (1–20) is considered only at some frequencies to keep the figure readable).
- The fact that Q_M (1–5) is very close to Q_{MoM} is very interesting from the engineering point of view-no matter where the feeding is located, the summation of the first five modes is sufficient enough to obtain accurate Q_M in the "low ka" region.

One minimum of total Q is located in the small antenna regime (for $ka = 0.736$, that is the resonant frequency of the first mode). Then the total Q rises to a value of about 350. As will be shown later, total Q can be effectively reduced in relatively broadband regions.

From Fig. 21 is also obvious that the total Q_M for a growing number of modes ($M = 1, \ldots, M = 5$) is increasingly better matched with Q_{MoM}. In fact, the Q_M factor is perfectly adjusted at natural resonances because there is only one significant entry of the $\boldsymbol{\beta}$ matrix (for example it is β_2 for $ka = 1.2$ at Fig. 21).

Including all β entries (not only the diagonal ones) is generally necessary for correct calculation. Compare the red solid line at Fig. 22 (which shows full summation where all members are used) with blue dashed lines (which consider only the diagonal terms of the $\boldsymbol{\beta}$ matrix). For simple structures (like a dipole), it is usually sufficient to use the self coupling diagonal terms, but generally energies produced by eigencurrents seem to be non orthogonal (unlike radiated powers).

2) Total Q_M Minimization: The following subsection draws out some benefits of the proposed method. We choose $ka = 1$ with $Q_M = 298.9$, see Figs. 20–22. Using optimization we now try to minimize the Q_M factor in the neighborhood of the selected point $ka = 1$ (which is the boundary value of ESA).

A significant advantage is that the TCM solution and ergo the modal energies $\mathbf{W}_e$ and $\mathbf{W}_m$ are computed only once. All single-calculated operations (eigensolution (13), 60 freq. samples, time: 229 s; tracking [30], 20 modes, time: 10 s; and modal energies calculation (3), (4), 5 modes, time: 62 s) took totally[5] 301 s. Our in-house Particle Swarm Optimization algorithm [32] is utilized to find optimal feeding scenarios—we consider two (voltage) gaps with independent magnitudes $E^i_{1/2} \in (0, 100)$V that may be located at any inner edges.

Equations (25) and (37) form the so-called fitness function (f.f.) which was evaluated for 50 agents and 300 iterations. Optimization takes a total of 1741 seconds which is only 0.116 second per f.f. call.

The original and the optimized feeding points are depicted at Fig. 23, together with the $\boldsymbol{\beta}$ matrices before and after optimization. Note here that the modal energies as well as the radi-

---

[5]All calculations presented in this paper were performed at computer with i7-X980 3.33 GHz processor, 24 GB RAM and SDD disc. As mentioned above, some processes were parallelized (with 8 threads).

ated power matrices are the same in both cases. The resulting impressed gap magnitudes are identical 80 V. The total Q_M is significantly decreased to the value $Q_M = 84.3$ at $ka = 1$. The optimized Q_M is shown at Fig. 22 as a black dashed line with an asterisk mark at the studied value of ka.

VI. CONCLUSION

Rigorous expressions for electric and magnetic stored energies are utilized for the evaluation of the radiation Q factor based on the superposition of the characteristic mode currents. It is demonstrated that the newly derived coupling matrix $\beta_{u,v}$ (that includes the frequency and the feeding effects) determines the total radiation factor Q_M. This matrix may be viewed as a connection between the intrinsic behaviour of the antenna (described by the set of characteristic currents) and the external world, represented by feeding.

The presented algorithm is implemented and verified for several examples. An up-to-date tracker is applied for sorting the modal data obtained from paralleled eigen-decomposition. Good agreement between the proposed summation technique and conventional methods is observed. All the examples clearly illustrate that the novel expressions together with the robust modal method can be used for the investigation of the modal and total Q factors.

The method stated above can be used for effective design of multiband and broadband ESAs. It also provides a deep physical insight into the studied structures. The commonly used Q_Z factor gives a nice estimation of the radiation Q, but it only answers the question "what is the overall Q?" In turn, the Q_M approach is much more general since answers also on important question "what might the overall Q be?" The presented concept opens novel possibilities for lowering the Q by using multipoint feeds and the design of MIMO antennas. The presented method has been successfully employed in the optimization loop as well. Further work is aimed to study complex planar geometries and detailed analysis of the exact relationship between (modal) radiation factors and maximum bandwidth.

APPENDIX
SUM OF MODAL ENERGIES

Consider (23) with M modes expressed as a double sum

$$W_{e/m}^M = \sum_{u=1}^{M} \sum_{v=1}^{M} \alpha_u \alpha_v^* W_{e/m}^{u,v}(\mathbf{J}_u, \mathbf{J}_v, q_u, q_v) \quad (40)$$

where modal energies $W_{e/m}^{u,v}(\dots)$ are calculated by (3), (4). In the following, the arguments of energies $W_{e/m}^{u,v}$ are omitted. The (40) may be divided into two parts

- $u = v$

  The term $\alpha_u \alpha_v^*$ is real and equal (see (15)) to

$$\alpha_u \alpha_v^* = \frac{\langle \mathbf{j}_u, \mathbf{E}^i \rangle^2}{1 + \lambda_u^2}. \quad (41)$$

If we expand the product (41) by $(1 + \lambda_u^2)$, then

$$W_{e/m}(u,u) = \sum_{u=1}^{M} \frac{\langle \mathbf{j}_u, \mathbf{E}^i \rangle^2 (1 + \lambda_u^2)}{(1 + \lambda_u^2)^2} W_{e/m}^{u,u}. \quad (42)$$

- $u \neq v$

  Since $\Re\{\alpha_u \alpha_v^*\} = \Re\{\alpha_u^* \alpha_v\}$, $\mathfrak{F}\{\alpha_u \alpha_v^*\} = -\mathfrak{F}\{\alpha_u^* \alpha_v\}$ and $W_{e/m}^{u,v} = W_{e/m}^{v,u}$ we can sum two terms at a time

$$W_{e/m}(u,v) + W_{e/m}(v,u) = (\alpha_u \alpha_v^* + \alpha_u^* \alpha_v) W_{e/m}^{u,v} \quad (43)$$

and from (15) after several manipulations

$$W_{e/m}(u,v) + W_{e/m}(v,u) = \frac{2\langle \mathbf{j}_u, \mathbf{E}^i \rangle \langle \mathbf{j}_v, \mathbf{E}^i \rangle (1 + \lambda_u \lambda_v)}{(1 + \lambda_u^2)(1 + \lambda_v^2)} W_{e/m}^{u,v}. \quad (44)$$

Using (42) and (44)

$$W_{e/m}^M = \sum_{u=1}^{M} \sum_{v=1}^{M} \frac{\langle \mathbf{j}_u, \mathbf{E}^i \rangle \langle \mathbf{j}_v, \mathbf{E}^i \rangle (1 + \lambda_u \lambda_v)}{(1 + \lambda_u^2)(1 + \lambda_v^2)} W_{e/m}^{u,v}. \quad (45)$$

REFERENCES

[1] J. L. Volakis, Ch.-Ch. Chen, and K. Fujimoto, "Survey of small antenna theory," in *Small Antennas: Miniaturization Techniques & Applications*, 1st ed. New York: McGraw-Hill, 2010, ch. 2, pp. 3–100.
[2] A. D. Yaghjian and S. R. Best, "Impedance, bandwidth and Q of antennas," *IEEE Trans. Antennas Propag.*, vol. 53, no. 4, pp. 1298–1324, Apr. 2005.
[3] H. A. Wheeler, "Fundamental limitations of small antennas," in *Proc. IRE*, Dec. 1947, vol. 35, pp. 1479–1484.
[4] L. J. Chu, "Physical limitations of omni-directional antennas," *J. Appl. Phys.*, vol. 19, pp. 1163–1175, Dec. 1948.
[5] R. F. Harrington, "Effect of antenna size on gain, bandwidth, and efficiency," *J. Res. Nat. Bur. Standards*, vol. 64D, pp. 1–12, Jan.–Feb. 1960.
[6] R. E. Collin and S. Rotchild, "Evaluation od antenna Q," *IEEE Trans. Antennas Propag.*, vol. 12, pp. 23–27, Jan. 1964.
[7] J. S. McLean, "A re-examination of the fundamental limits on the radiation q of electrically small antennas," *IEEE Trans. Antennas Propag.*, vol. 44, pp. 672–675, May 1996.
[8] Y. Geyi, "A method for the evaluation of small antenna Q," *IEEE Trans. Antennas Propag.*, vol. 51, pp. 2124–2129, Aug. 2003.
[9] M. Gustafsson, C. Sohl, and G. Kristensson, "Physical limitations on antennas of arbitrary shape," in *Proc. Royal Society A: Mathematical, Physical and Engineering Sciences*, 2007, vol. 463, no. 2086, pp. 2589–2607.
[10] G. A. E. Vandenbosch, "Reactive energies, impedance, and Q factor of radiating structures," *IEEE Trans. Antennas Propag.*, vol. 58, no. 4, pp. 1112–1127, Apr. 2010.
[11] P. Hazdra, M. Capek, and J. Eichler, "Radiation Q-factors of thin-wire dipole arrangements," *IEEE Antennas Wireless Propag. Lett.*, vol. 10, pp. 556–560, May 2011.
[12] R. F. Harrington and J. R. Mautz, "Theory of characteristic modes for conducting bodies," *IEEE Trans. Antennas Propag.*, vol. 19, no. 5, pp. 622–628, Sept. 1971.
[13] R. F. Harrington, *Field Computation by Moment Methods*. New York: John Wiley—IEEE Press, 1993.
[14] K. F. Warnick, *Numerical Analysis for Electromagnetic Integral Equations*. Norwood, MA: Artech House, 2008.
[15] C. A. Balanis, *Advanced Engineering Electromagnetics*. New York: Wiley, 1989.
[16] P. Hazdra and P. Hamouz, "On the modal superposition lying under the MoM matrix equations," *Radioengineering*, vol. 17, no. 3, pp. 42–46, Sep. 2008.
[17] W. C. Gibson, *The Method of Moments in Electromagnetics*, 1st ed. London, U.K.: Chapman & Hall, 2008.
[18] R. F. Harrington and J. R. Mautz, "Computation of characteristic modes for conducting bodies," *IEEE Trans. Antennas Propag.*, vol. 19, no. 5, pp. 629–639, Sept. 1971.

[19] S. M. Rao, D. R. Wilton, and A. W. Glisson, "Electromagnetic scattering by surfaces of arbitrary shape," *IEEE Trans. Antennas Propag.*, vol. 30, no. 3, pp. 409–418, May 1982.

[20] M. Cabedo-Fabres *et al.*, "The theory of characteristic modes revisited: A contribution to the design of antennas for modern applications," *IEEE Antennas Propag. Mag.*, vol. 49, no. 5, pp. 52–68, Oct. 2007.

[21] E. Anderson *et al.*, *LAPACK Users' Guide*. Philadelphia, PA: Society for Industrial and Applied Mathematics (SIAM), 1999.

[22] M. Cabedo-Fabres, "Systematic Design of Antennas Using the Theory of Characteristic Modes," Ph.D. dissertation, UPV, Spain, Feb. 2007.

[23] R. A. Horn and C. R. Johnson, *Topics in Matrix Analysis*. Cambridge, U.K.: Cambridge Univ. Press, 1994.

[24] S. N. Makarov, *Antenna and EM Modeling with Matlab*, 1st ed. New York: John Wiley, 2002.

[25] P.-O. Persson, "Mesh Generation for Implicit Geometries," PhD. Thesis, MIT, , 2005.

[26] E. H. Newman, "Small antenna location synthesis using characteristic modes," *IEEE Trans. Antennas Propag.*, vol. 27, no. 4, pp. 530–531, July 1979.

[27] J. F. Shaeffer, MOM3D Method of Moments Code Theory Manual Denmar, Marietta, Georgia, Contract NAS1-18603, Rep. 189594, Mar. 1992.

[28] T. F. Eibert and V. Hansen, "On the calculation of potential integrals for linear source distributions on triangular domains," *IEEE Trans. Antennas Propag.*, vol. 43, no. 12, pp. 1499–1502, Dec. 1995.

[29] P. Arcioni, M. Bressan, and L. Perregrini, "On the evaluation of the double surface integrals arising in the application of the boundary integral method to 3-D problems," *IEEE Trans. Microwave Theory Tech.*, vol. 45, no. 3, pp. 436–439, Mar. 1997.

[30] M. Capek, P. Hazdra, P. Hamouz, and J. Eichler, "A method for tracking characteristic numbers and vectors," *Progr. Electromagn. Res. B*, vol. 33, pp. 115–134, 2011.

[31] R. F. Harrington and J. R. Mautz, "Control of radar scattering by reactive loading," *IEEE Trans. Antennas Propag.*, vol. 20, no. 4, pp. 446–454, Jul. 1972.

[32] M. Capek, P. Hazdra, P. Hamouz, and M. Mazanek, "Software tools for efficient generation, modeling and optimisation of fractal radiating structures," *IET Microw., Antennas Propag.*, vol. 5, no. 8, pp. 1002–1007, Jun. 2011.
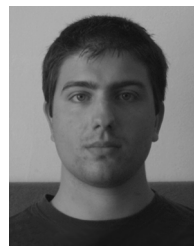
Miloslav Capek (S'09) received the M.Sc. degree in electrical engineering from the Czech Technical University, Prague, Czech Republic, in 2009, where he is currently working towards the Ph.D. degree.

His research interests are in the area of electrically small antennas, numerical techniques, fractal geometry and optimalization.

Pavel Hazdra (M'03) received the M.S. and Ph.D. degrees in electrical engineering from the Czech Technical University in Prague, in 2003 and 2009, respectively.

He is a Research and Teaching Assistant with the Department of Electromagnetic Field, CTU-FEE. His research interests are in the area of electromagnetic theory, computational electromagnetics, fractal geometry, planar antennas and special prime-feed antennas.

Jan Eichler (S'10) received the B.Sc. and M.Sc. degrees in electrical engineering from the Czech Technical University in Prague, in 2008 and 2010, respectively, where he is currently working towards the Ph.D. degree.

His research interests include multiband antennas, their simulation (full-wave or modal), fractal motifs and the quality factor of an antenna.